eLIFE elifesciences.org

RESEARCH ARTICLE

Figures and figure supplements

Epithelial magnesium transport by TRPM6 is essential for prenatal development and adult survival

Vladimir Chubanov *et al*

A

Stage	Embryos isolated	*Trpm6*$^{\beta geo/\beta geo}$ embryos
e8.5	15	3
e9.5	13	5
e10.5	8	2
e11.5	8	1
e12.5	17	1
e14.5	18	0
After e14.5	21	0

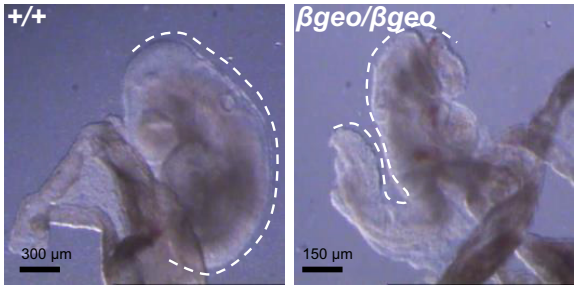

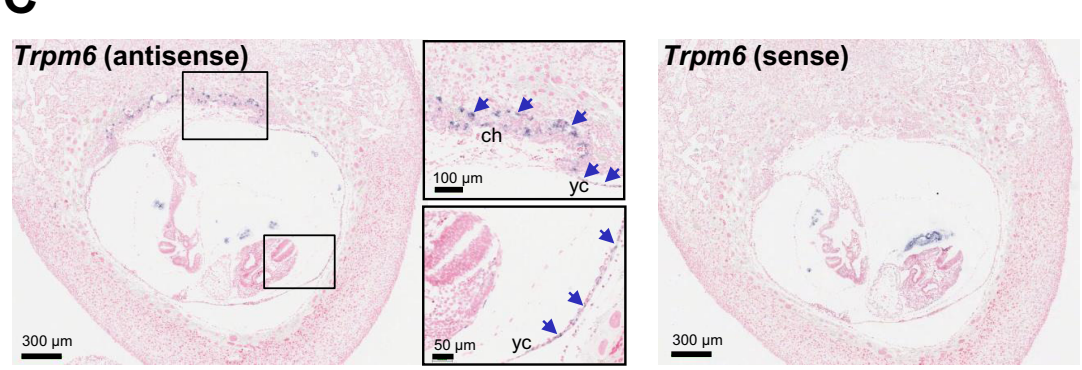

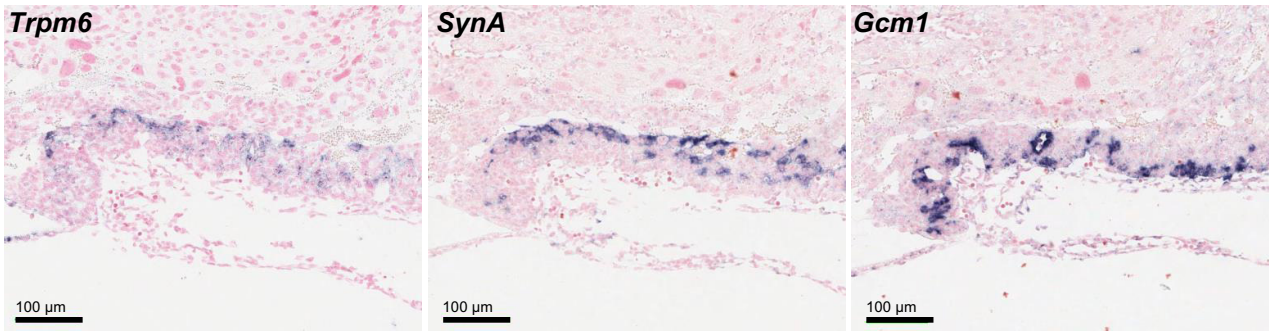

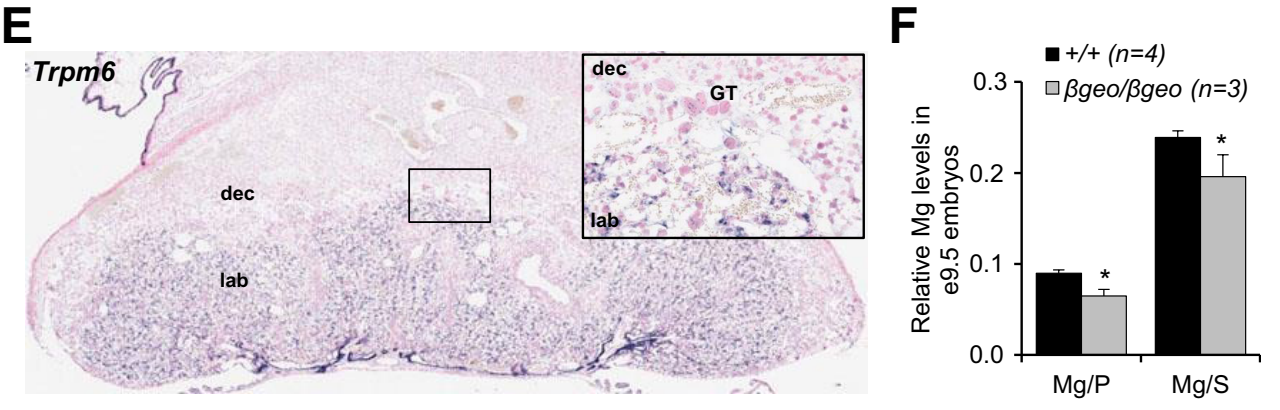

Figure 1. Assessment of *Trpm6* function in extraembryonic tissues. (**A**) Survival of *Trpm6*$^{\beta geo/\beta geo}$ embryos obtained from *Trpm6*$^{\beta geo/+}$ intercrosses. (**B**) Representative images of e9.5 *Trpm6*$^{+/+}$ (*+/+*, n = 13) and *Trpm6*$^{\beta geo/\beta geo}$ (*βgeo/βgeo*, n = 5) embryos from dataset in (**A**). Dashed lines underline C-

Figure 1 continued on next page

Figure 1 continued

shaped versus S-shaped morphology of *Trpm6*$^{+/+}$ and *Trpm6*$^{\beta geo/\beta geo}$ embryos, respectively. (**C**) ISH on serial paraffin sections obtained from wildtype n = 5 e8.5 fetus using antisense (left) and sense (right) probes for *Trpm6*. Boxes indicate the positions of the magnified images of the chorion (*ch*) and yolk sac (*yc*). Arrows indicate *Trpm6*-positive cells in the developing labyrinth (chorion) and the endoderm layer in the visceral yolk sac. (**D**) ISH on serial paraffin sections of wildtype e8.5 placenta using DIG-labelled probes for *Trpm6* (*left*), *SynA* (*middle*) and *Gcm1* (*right*), respectively. *Note: Trpm6* expression was restricted to cells positive for *SynA*, a marker of SynT-I, and absent in cells expressing *Gcm1*, a marker of SynT-II. Representative images of n = 2 independent tissues are shown. (**E**) ISH of WT e14.5 placenta with the antisense *Trpm6* probe. The box indicates the position of the magnified image. The *Trpm6* signal is restricted to the labyrinth (*lab*) and not detectable in the decidua (*dec*) and trophoblast giant cells (GT). Representative images of n = 8 independent placentas are shown. (**F**) Mg^{2+} levels in e9.5 *Trpm6*$^{+/+}$ (n = 4) and *Trpm6*$^{\beta geo/\beta geo}$ (n = 3) embryos. Distal segments of the embryos were used for genotyping, and the remaining parts were analysed by ICP-MS. Elementary magnesium (Mg) contents were normalized to phosphorus (P) and sulfur (S) levels represented as mean±SEM. *-p≤0.05 (Student's t-test).

DOI: 10.7554/eLife.20914.003

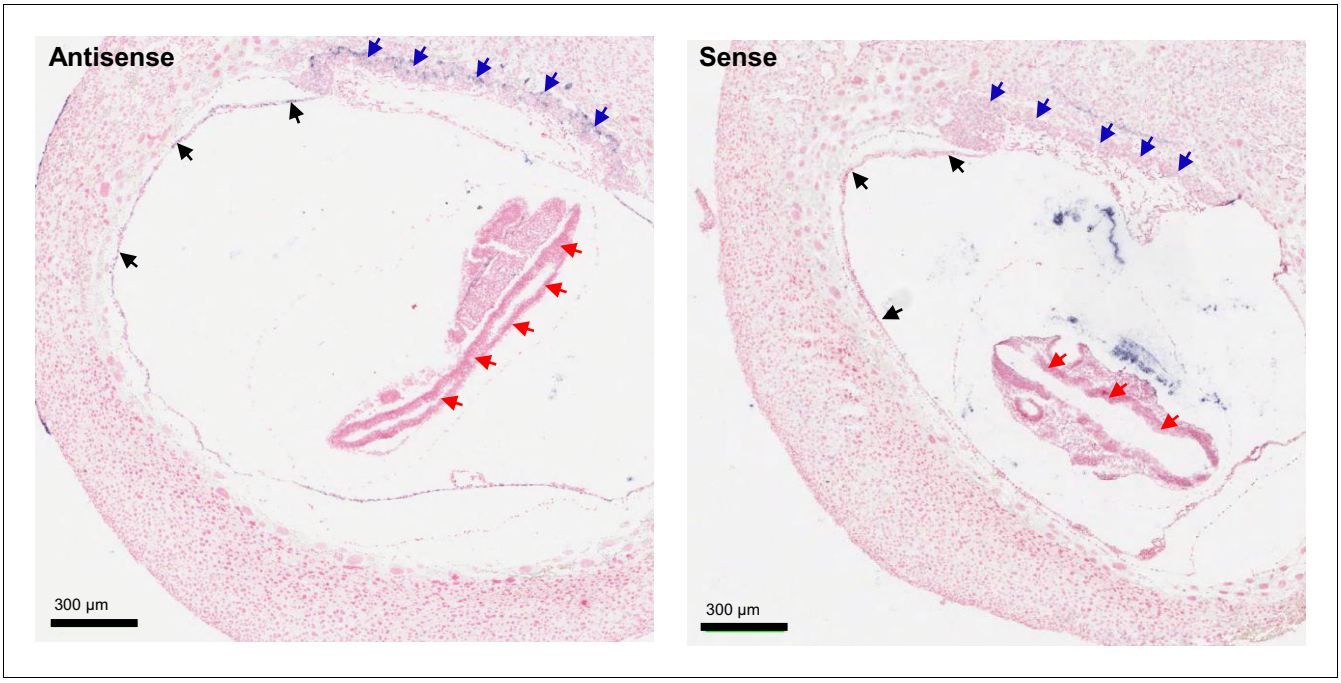

Figure 1—figure supplement 1. ISH on serial paraffin sections obtained from wildtype e8.5 fetus using antisense (left) and sense (right) probes for *Trpm6*. Arrows indicate *Trpm6*-positive cells in the chorion (blue arrows) and the endoderm layer in the visceral yolk sac (black arrows) stained only by the antisense probe. Note: *Trpm6* was not detectable in embryonic tissues including the neural tube (red arrows).
DOI: 10.7554/eLife.20914.004

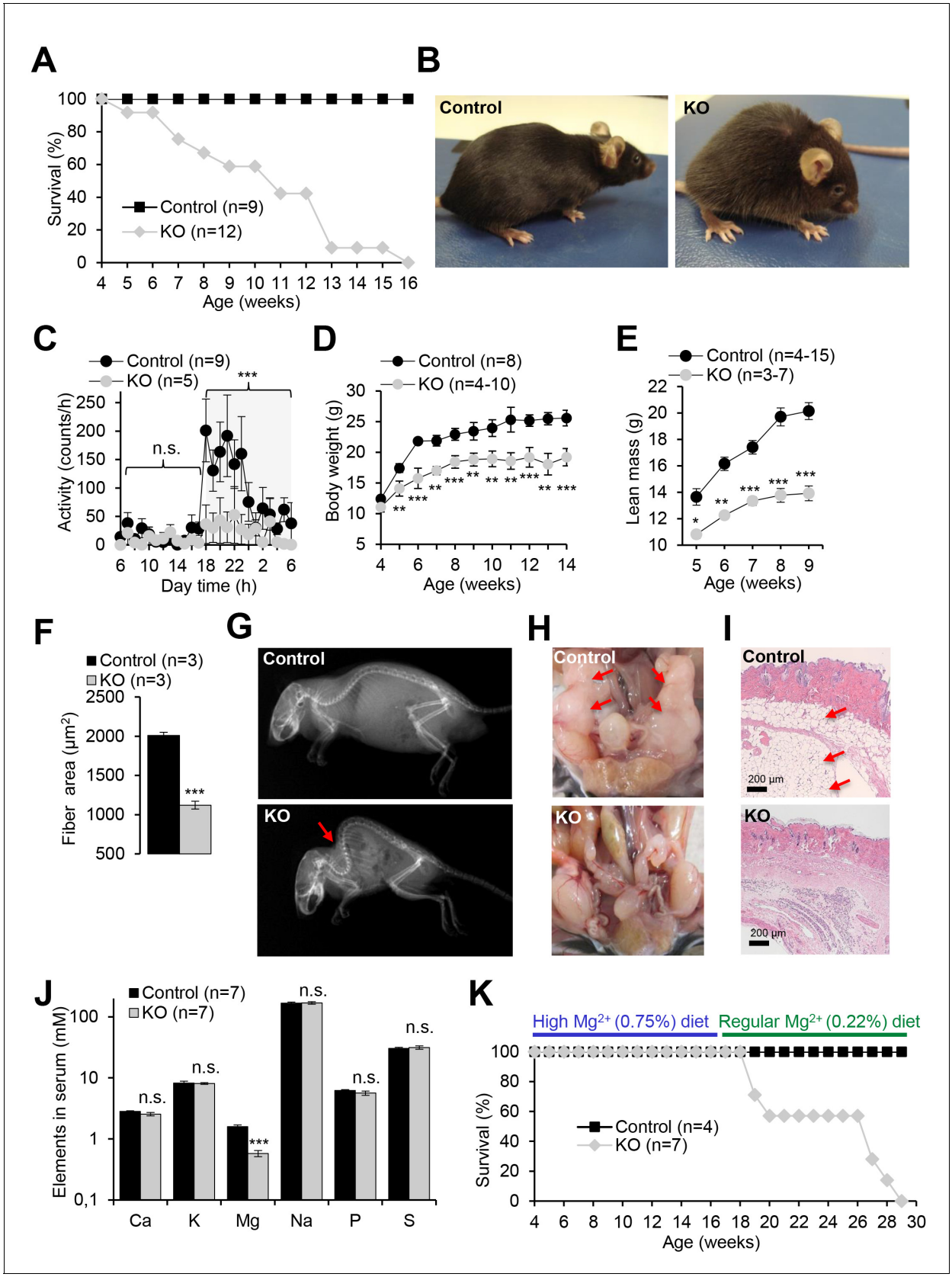

Figure 2. Pathophysiological changes displayed by *Trpm6*-deficient adult mice. Unless stated otherwise, 10–12 week-old *Trpm6*$^{fl/+}$ (*Control*) and *Trpm6*$^{\Delta 17/\Delta 17}$;*Sox2-Cre* (*KO*) littermates were studied. (**A–E**) Mice were examined for survival rate (**A**), overall physical appearance (**B**), day/night activity

Figure 2 continued on next page

Figure 2 continued

of 8 week-old individuals (**C**), growth rate (**D**) and lean mass (**E**). (**F**) Fibre size of the gastrocnemius muscle after hematoxylin-eosin staining. (**G**) X-ray images of mice. The red arrow indicates the characteristic skeletal deformation (kyphosis) observed in *Trpm6*-deficient mice. (**H**) Assessment of abdominal fat. Arrows indicate fat deposits observed only in control mice. (**I**) H and E staining of paraffin skin sections. Arrows indicate a layer of fat cells present only in control mice. Histological analysis was performed with three animals per group resulting in similar observations. (**J**) The levels of main elements in the serum of 8 week-old mice assessed by ICP-MS. (**K**) The survival rate of mice maintained on high Mg^{2+} (0.75%) and regular (0.22%) chows. Data are represented as mean±SEM. ***-$p \leq 0.001$; **-$p \leq 0.01$; *-$p \leq 0.05$; n.s. – not significantly different (Student's t-test); n – number of mice examined.

DOI: 10.7554/eLife.20914.006

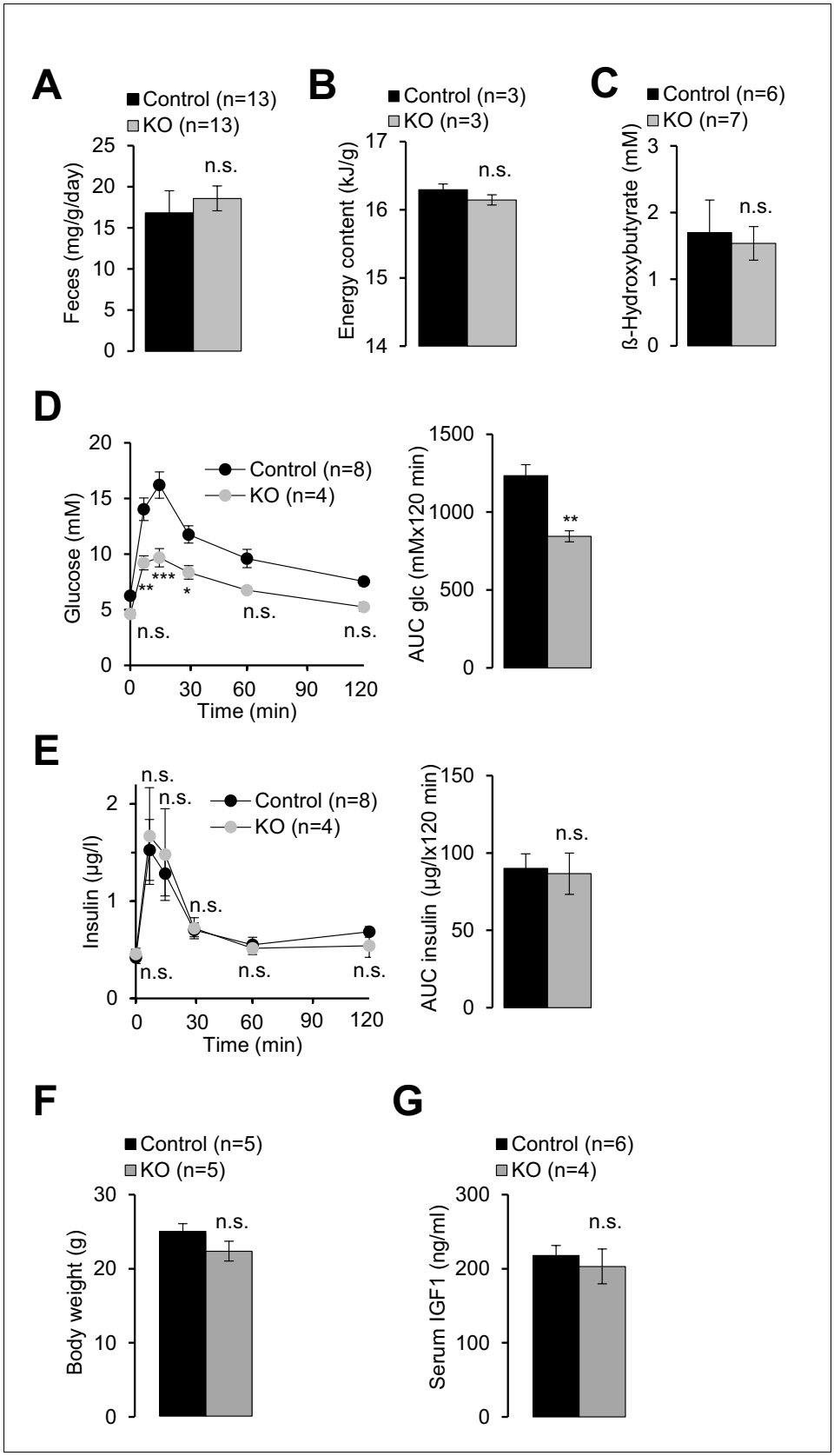

Figure 2—figure supplement 1. Examination of energy balance in *Trpm6*-deficient mice. Eight week-old *Trpm6*$^{fl/+}$ (*Control*) and *Trpm6*$^{\Delta 17/\Delta 17}$;*Sox2-Cre* (*KO*) littermates were evaluated for (**A**) chow intake as assessed by

Figure 2—figure supplement 1 continued on next page

Figure 2—figure supplement 1 continued

feces production, (**B**) energy content of feces studied by bomb calorimetry and (C) serum levels of β-hydroxybutyrate. Glucose (**D**) and insulin levels (**E**) in the serum of mice subjected to a glucose tolerance test. *Note:* mutant mice had lower peripheral glucose concentrations than controls despite of a similar amount of insulin released, thus reflecting increased insulin sensitivity. Data are represented as mean±SEM. ***-$p \leq 0.001$; **-$p \leq 0.01$; *-$p \leq 0.05$; n.s. – not significantly different (Student's t-test); n – number of mice examined.
DOI: 10.7554/eLife.20914.007

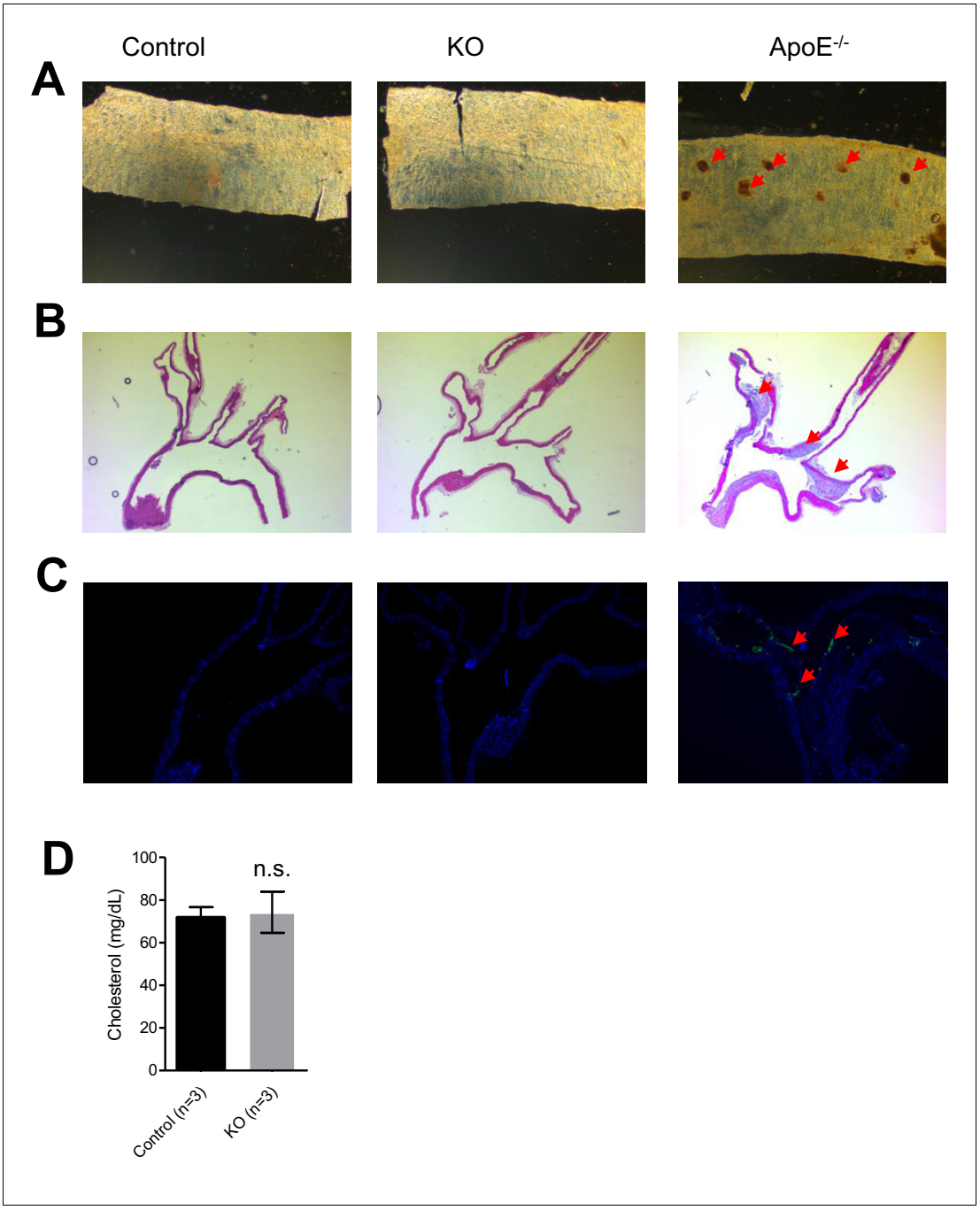

Figure 2—figure supplement 2. Evaluation of atherosclerosis development in *Trpm6*-deficient mice. An assessment of 8 week-old control (*Control*, n = 3) and *Trpm6*-deficient (*KO*, n = 3) with *ApoE*$^{-/-}$ mice (as a positive control, n = 1) using en-face thoracal aorta preparation and Oil-Red O staining (**A**) and hematoxylin-eosin staining (**B**), Mac2-staining (green) (**C**) of aortic arches. Representative images are shown. Arrows indicate atherosclerosis lesions observed only in *ApoE*$^{-/-}$ mice. (**D**) Plasma cholesterol levels (mean±SEM) of control and *Trpm6*-deficient mice. n.s. – not significantly different (Student's t-test); n – number of mice examined.

DOI: 10.7554/eLife.20914.008

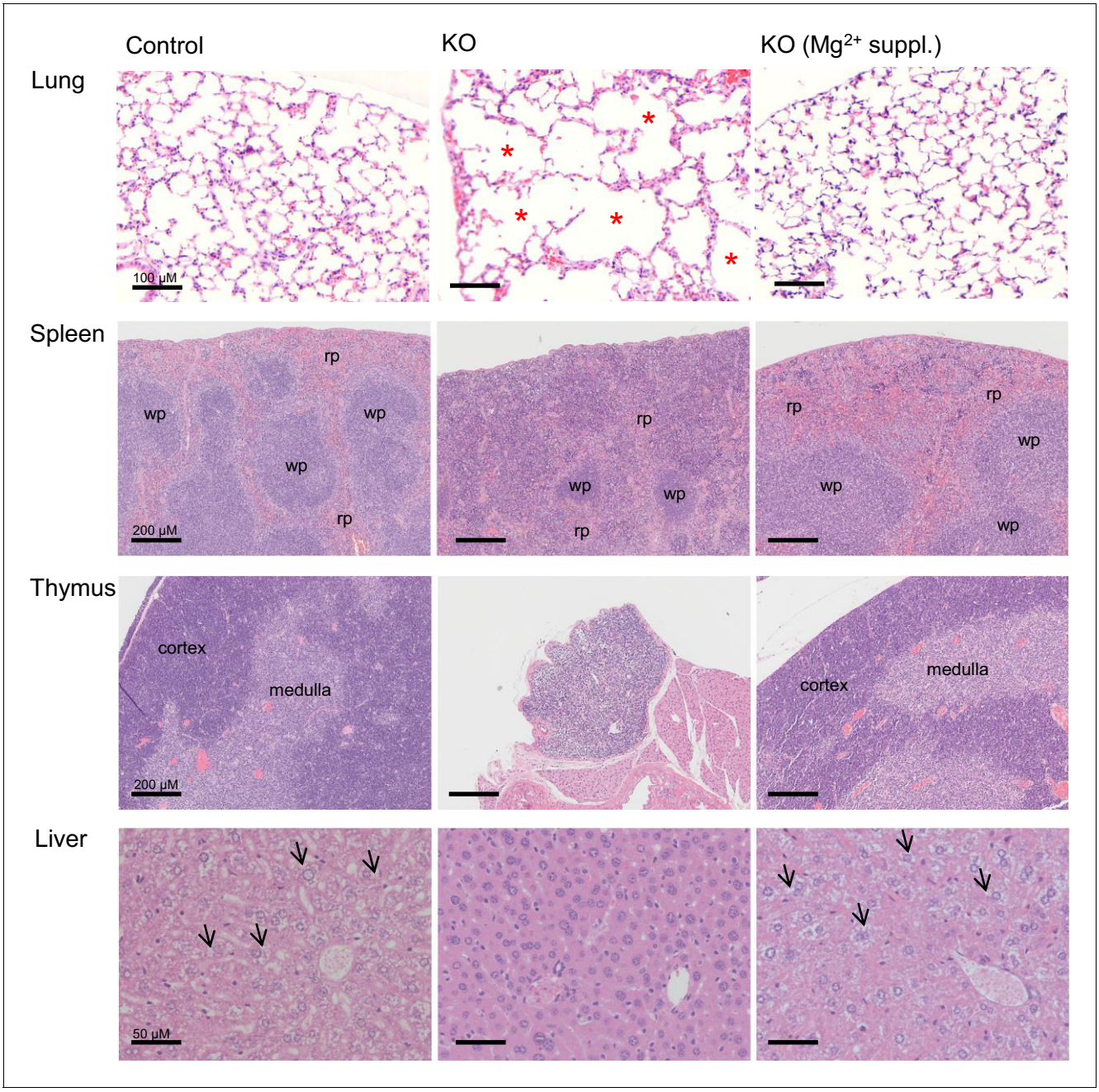

Figure 3. Histology of internal organs of *Trpm6*-deficient mice. Hematoxylin-eosin staining of paraffin embedded tissue sections of 12–13 week-old control (*Control*) and *Trpm6*-deficient (*KO*) mice maintained either on regular (0.22% Mg^{2+}) or Mg^{2+} supplemented (0.75% Mg^{2+}) chows. *Trpm6*-deficient mice maintained on the regular diet showed marked airspace enlargement (indicated by stars) mimicking lung emphysema, distortion of splenic red pulp (*rp*)/ white pulp (*wp*) microarchitecture, thymic atrophy, and reduction of intracellular glycogen in hepatocytes (indicated by arrows). Histological analysis was performed with three animals per group resulting in similar observations.

DOI: 10.7554/eLife.20914.009

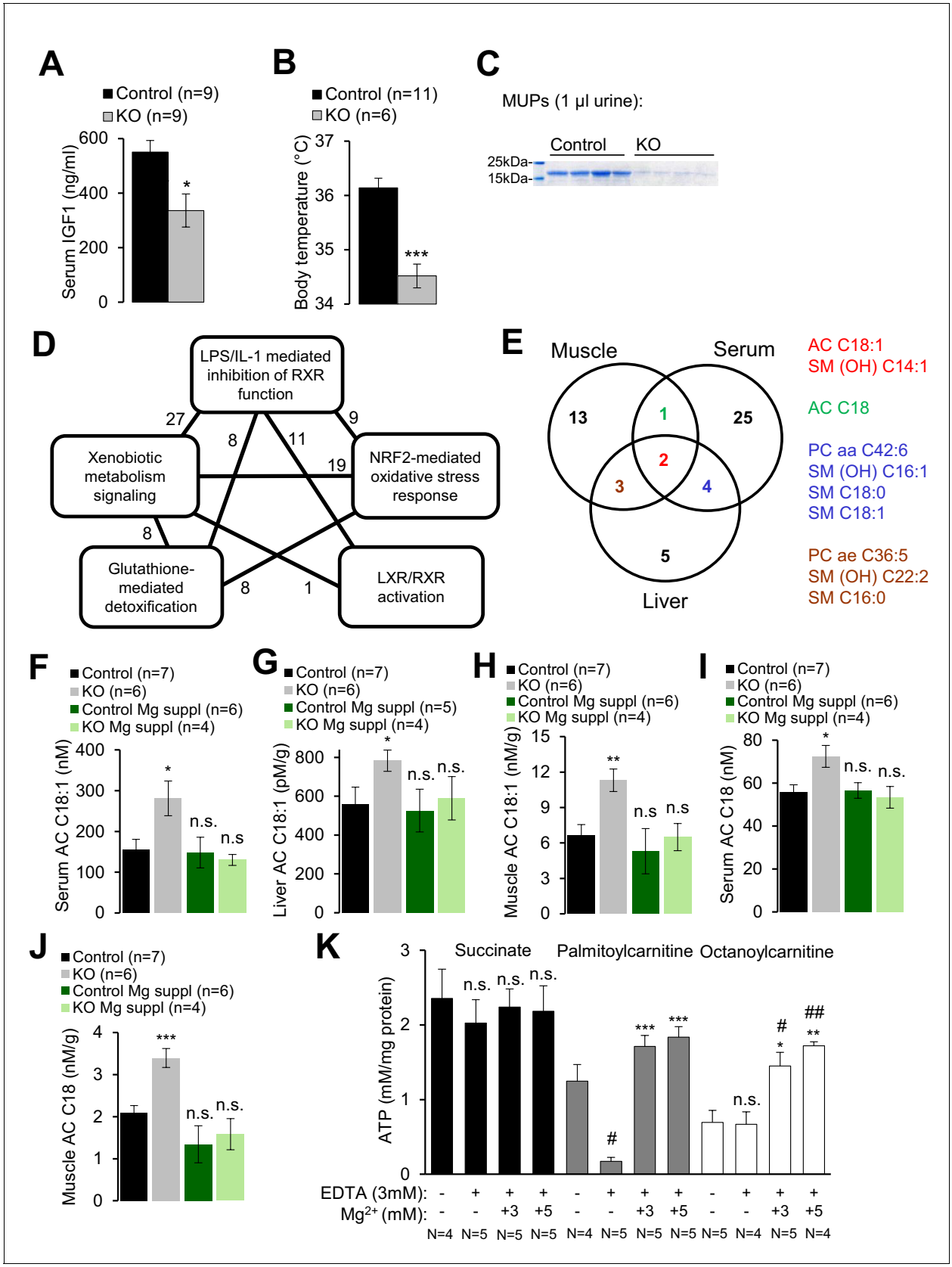

Figure 4. Assessment of metabolic profiles of *Trpm6*-deficient mice. (**A–C**) 8 week-old *Trpm6*$^{fl/+}$ (*Control*) and *Trpm6*$^{\Delta 17/\Delta 17}$;*Sox2-Cre* (*KO*) littermates were evaluated for (**A**) serum IGF1, (**B**) body temperature, (**C**) urinary MUPs content in individual mice. Data are represented as mean±SEM. ***-

Figure 4 continued on next page

Figure 4 continued

p≤0.001; *-p≤0.05 (Student's t-test); n – number of mice examined. (**D**) IPA analysis of genome-wide hepatic transcriptome profiling of *Trpm6*-deficient (n = 3) *vs* control (n = 4) littermates. The diagram shows the top 5 of IPA Canonical Pathways significantly changed in mutant mice (***Supplementary file 2***). Numbers of the commonly changed transcripts are indicated close to the lines connecting the pathways. (**E**) Venn diagram for sets of metabolites significantly changed (FDR p≤0.05) in serum, liver and gastrocnemius muscle *Trpm6*-deficient (n = 6) *vs* control (n = 8) littermates (***Supplementary file 3***). Commonly changed metabolites are listed in different colours as outlined in the Venn diagram. (**F–J**) Levels of AC C18:1 (**F–H**) and AC C18 (**I–J**) examined in the serum (**F, I**), liver (**G**) and gastrocnemius muscle (**H, J**) of *Trpm6*-deficient and control mice. Data are represented as mean±SEM. ***-p≤0.001; **-p≤0.01; *-p≤0.05; n.s. – not significantly different to control group maintained on a regular Mg^{2+} diet (one-way ANOVA); n – number of mice examined. (**K**) ATP production by mitochondria isolated from the liver of wildtype C57BL/6 mice with succinate, palmitoylcarnitine or octanoylcarnitine as energy sources. ATP levels were determined after 30 min incubation of untreated (-) or treated (+) mitochondria by EDTA with or without Mg^{2+}. Data are represented as mean±SEM of 4–5 independent isolations (**N**). $^{\#\#}$-p≤0.01; $^{\#}$-p≤0.05 significantly different to the control group; ***-p≤0.001; **-p≤0.01; *-p≤0.05 significantly different to the EDTA treated group (Student's t-test). n.s. – not significantly different.

DOI: 10.7554/eLife.20914.010

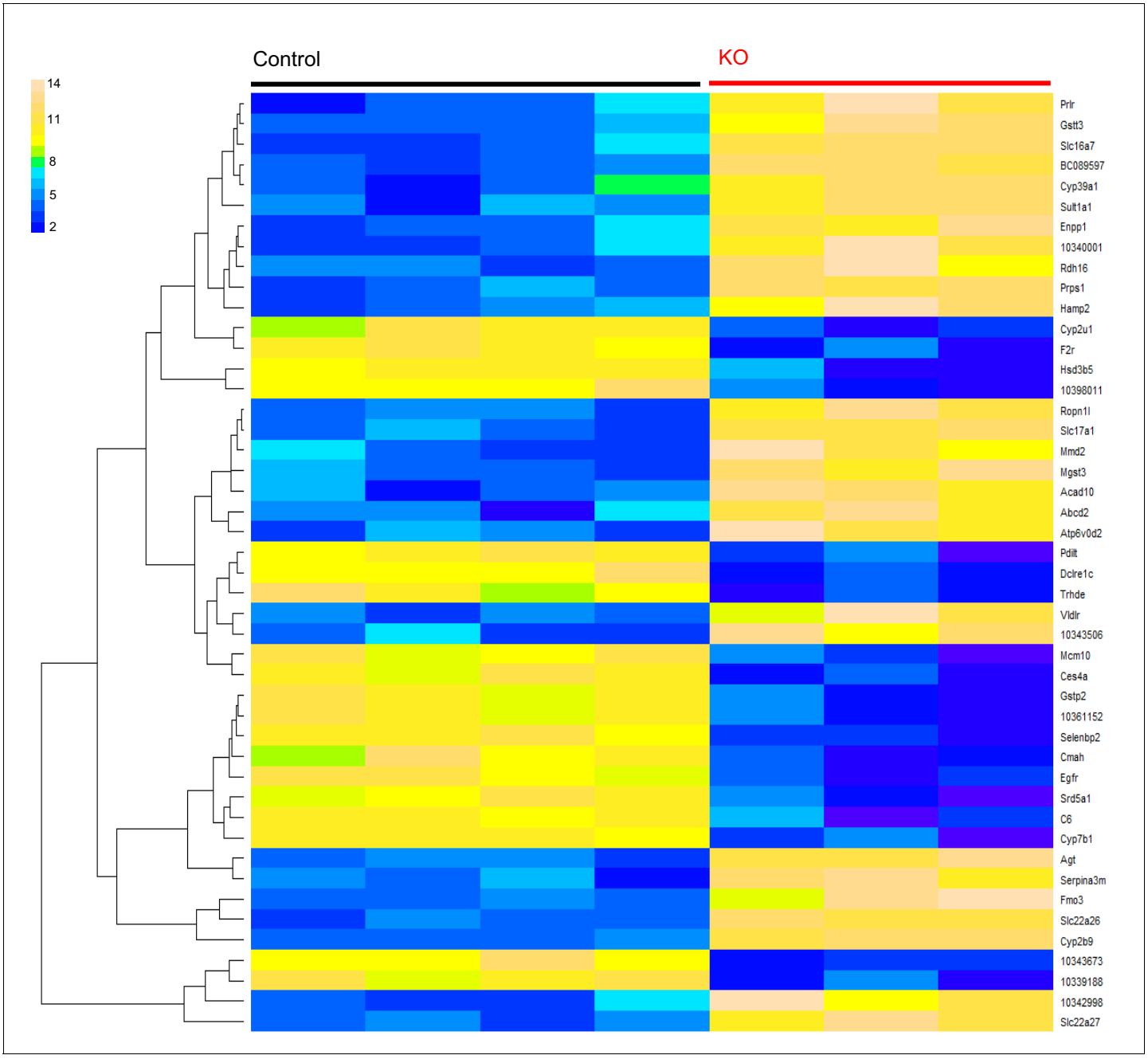

Figure 4—figure supplement 1. Gene expression profiling of *Trpm6*-deficient and control mice. Heatmap diagram of differently expressed genes with FDR p≤0.1 in the liver of 12–13 week-old control (*Trpm6*$^{fl/+}$, n = 4) *vs Trpm6*-deficient (*Trpm6*$^{\Delta 17/\Delta 17}$*;Sox2-Cre,* n = 3) male littermates. n – number of mice examined.

DOI: 10.7554/eLife.20914.011

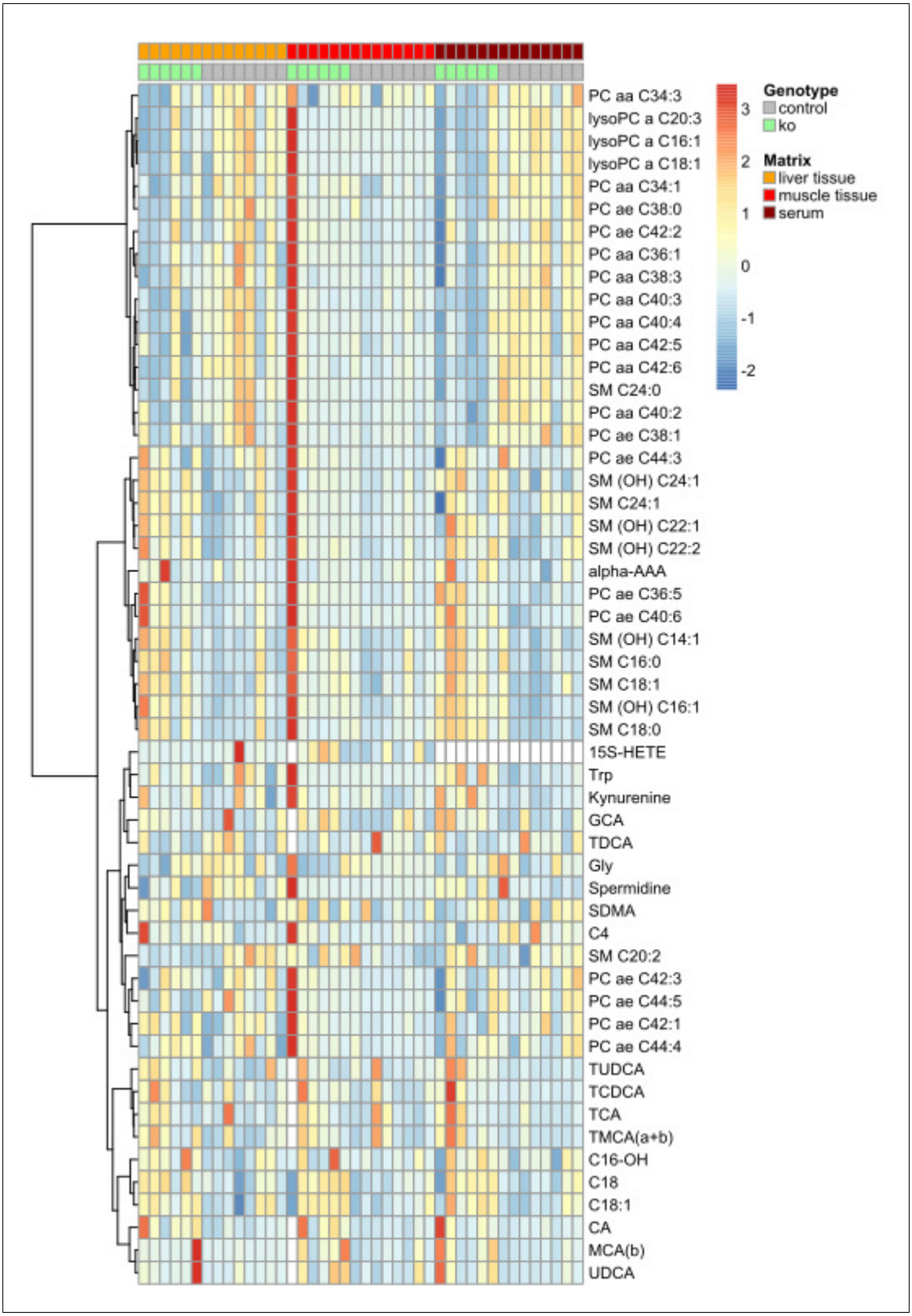

Figure 4—figure supplement 2. Metabolomic profiling of *Trpm6*-deficient and control mice. Profiling of metabolites in the serum, liver and gastrocnemius muscle samples from 8–10 week-old control (*Trpm6*$^{fl/+}$, n = 8) and KO (*Trpm6*$^{\Delta 17/\Delta 17}$;*Sox2-Cre*, n = 6) male littermates were studied for a

Figure 4—figure supplement 2 continued on next page

Figure 4—figure supplement 2 continued

panel of 237 metabolites outlined in ***Supplementary file 3***. The heatmap diagram shows concentration levels scaled to zero mean and unit standard deviation of significantly changed metabolites for control and KO genotypes in a colour-coded way. n – number of mice examined.
DOI: 10.7554/eLife.20914.012

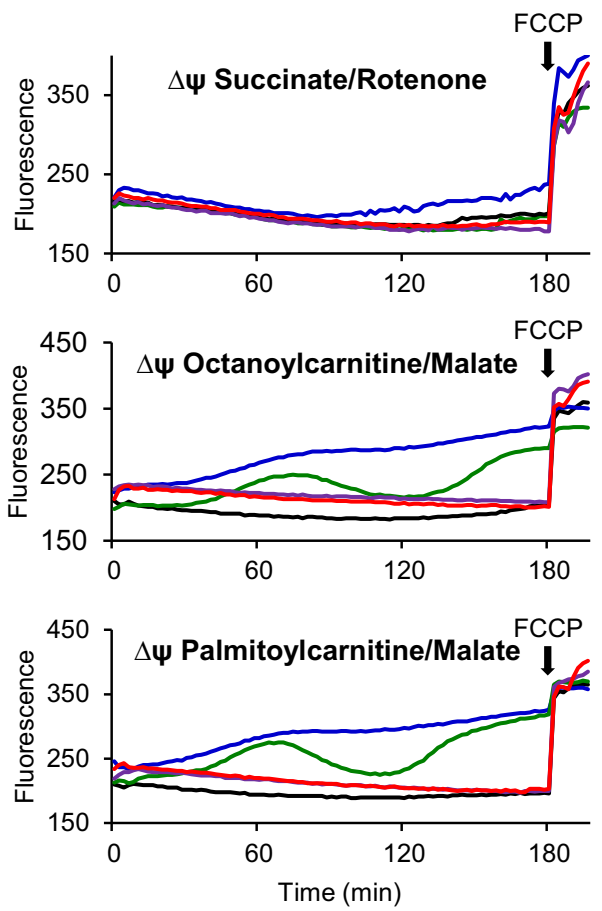

Depolarization start and end (min)

	+3 mM EDTA				
Mg^{2+}:	-	-	+1 mM	+3 mM	+5 mM
Legend					
N (n)	4 (6)	4 (6)	4 (6)	4 (6)	4 (6)
	Succinate/Rotenone				
Start	130 ± 19	≥ 180[a] **	158 ± 20 *#	≥ 180 **‡	≥ 180 **‡
End	≥ 180	≥ 180[a]	≥ 180	≥ 180	≥ 180
	Octanoylcarnitine/Malate				
Start	168 ± 14	19 ± 11 ***	31 ± 11 ***#	≥ 180 ###‡‡‡	≥ 180 ###‡‡‡
End	≥ 180	175 ± 6	178 ± 3	≥ 180	≥ 180
	Palmitoylcarnitine/Malate				
Start	157 ± 28	20 ± 7 ***	38 ± 13 ***	≥ 180 ###‡‡‡	≥ 180 ###‡‡‡
End	≥ 180	149 ± 42	≥ 180	≥ 180	≥ 180

[a] N=3, n=5.

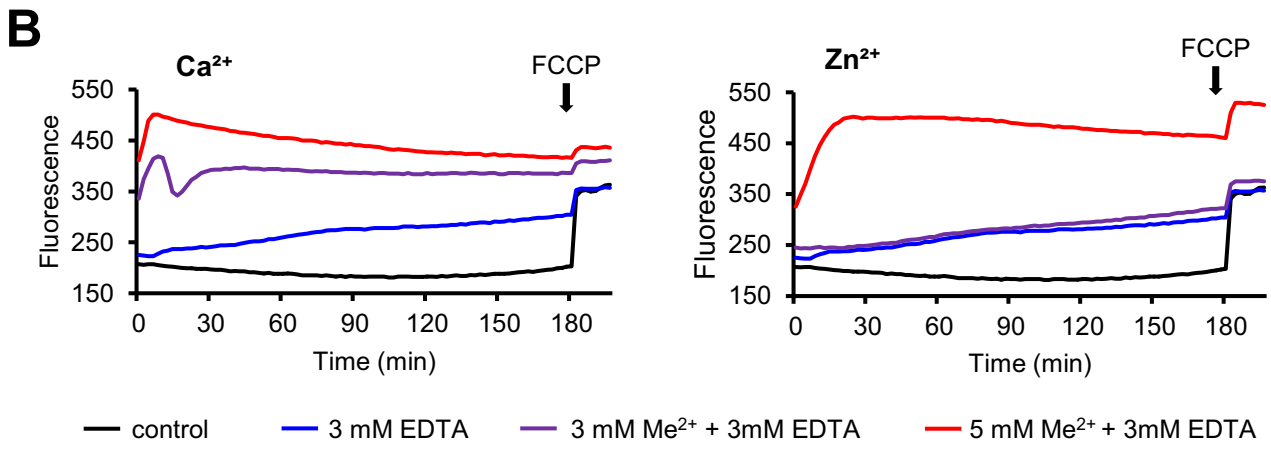

Figure 4—figure supplement 3. Assessment of the membrane potential ($\Delta\psi_m$) in isolated mitochondria. (**A**) Mitochondria isolated from the liver of wildtype C57BL/6 mice were incubated (30 min) in the presence of succinate/rotenone, octanoylcarnitine/malate or palmitoylcarnitine/malate as energy source. The *left panel* shows representative measurements of $\Delta\psi_m$ using Rh123 probe. As a positive control, carbonyl cyanide 4-(trifluoromethoxy) phenylhydrazone (FCCP) was added at the end of recording to induce breakdown of $\Delta\psi_m$. The *right panel* shows the calculated start- and endpoints of $\Delta\psi_m$ elicited by the application of 3 mM EDTA in the absence or presence of 1–5 mM Mg^{2+} for traces shown in *left panel*. Data are represented as mean±SD. N – independent mitochondria isolations; n – independent measurements. ***-p≤0.001, **-p≤0.01, *-p≤0.05 significant to the untreated

Figure 4—figure supplement 3 continued on next page

Figure 4—figure supplement 3 continued

(control) group; $^{###}$-p≤0.001, $^{##}$-p≤0.01, $^{#}$-p≤0.05 significant to 3 mM EDTA + 0 mM Mg^{2+} group; ‡‡‡-p≤0.001, ‡‡-p≤0.01, ‡-p≤0.05 significant to 3 mM EDTA + 1 mM Mg^{2+} group (Student's t-test). (**B**) Representative measurements of ψ_m in the presence of 3 mM EDTA with/without 3–5 mM Ca^{2+} or Zn^{2+} performed analogously to (**A**). Three independent experiments showed similar results.

DOI: 10.7554/eLife.20914.013

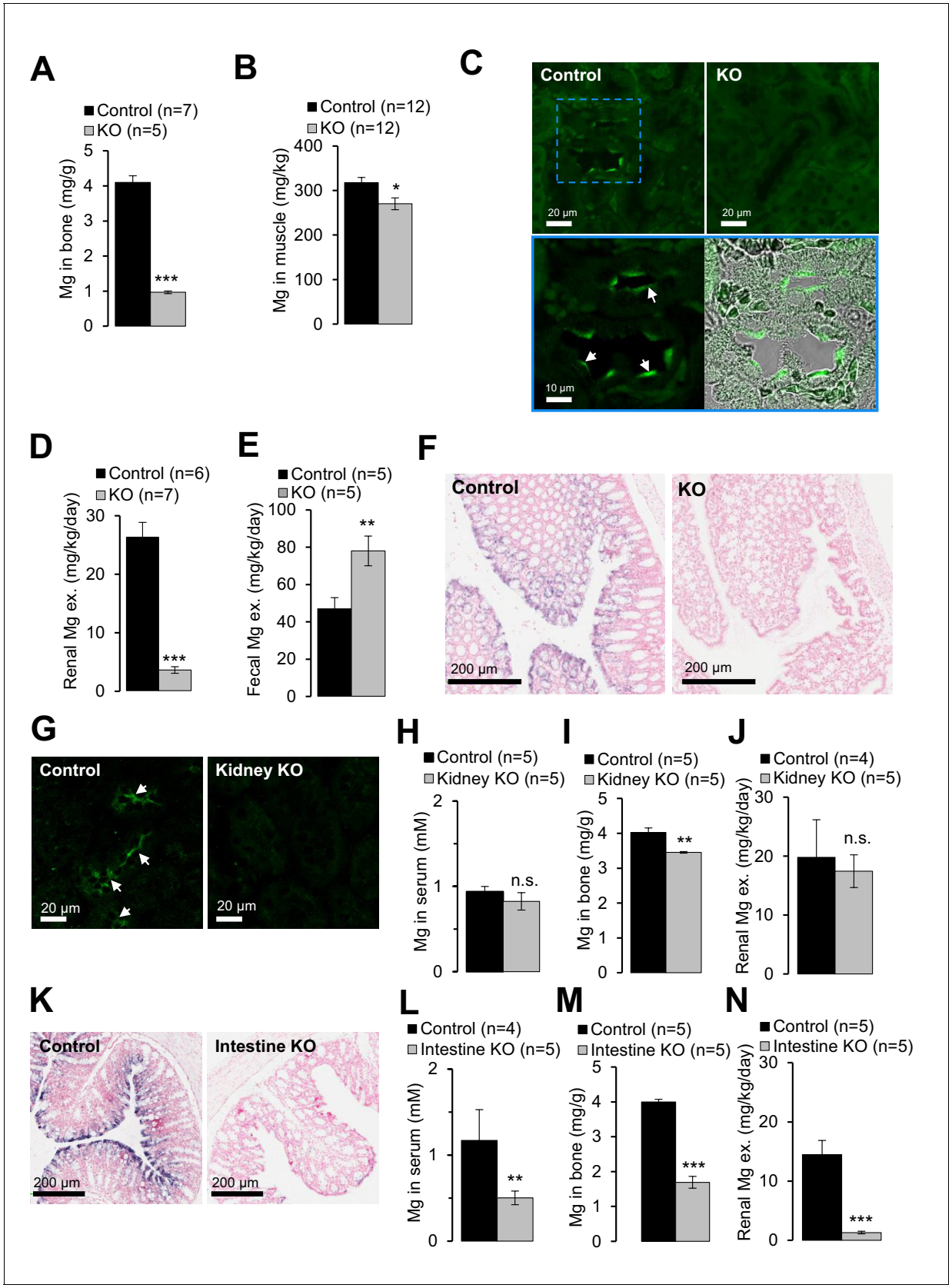

Figure 5. Examining of Mg^{2+} balance in *Trpm6*-deficient adult mice. (**A–F**) Assessment of 8 week-old *Trpm6*$^{fl/+}$ (*Control*) and *Trpm6*$^{\Delta 17/\Delta 17}$;*Sox2-Cre* (*KO*) littermate males. (**A**) Mg^{2+} levels in bones and (**B**) gastrocnemius muscle assessed by ICP-MS. (**C**) Immunostaining of kidney cryosections using a

Figure 5 continued on next page

Figure 5 continued

TRPM6-specific antibody. Representative images are shown (n = 2 tissues per genotype). The blue square indicates the position of the confocal and differential interference contrast magnified images acquired from control tissue. Arrows indicate labelling of the apical surface of renal tubules. (**D**) 24 hr urinary and (**E**) fecal Mg^{2+} excretion rates. (**F**) ISH on paraffin sections obtained from the colon of control and *Trpm6*-deficient mice (n = 2 tissues per genotype). (**G–J**) Examination of 6 month-old *Trpm6*$^{fl/+}$ (*Control*) and *Trpm6*$^{\Delta 17/fl}$*;Ksp-Cre* (*Kidney KO*) littermate males. (**G**) Immunostaining of TRPM6 in kidney cryosections. *Arrows* indicate labelling of renal tubules. (**H–I**) Determination of Mg^{2+} in serum (**H**) and bones (**I**). (**J**) 24 hr urinary Mg^{2+} excretion rate. (**K–N**) Assessment of 6 month-old *Trpm6*$^{fl/+}$ (*Control*) and *Trpm6*$^{\Delta 17/fl}$*;Villin1-Cre* (*Intestine KO*) littermate males. (**K**) ISH on paraffin sections of the colon using a *Trpm6*-specific probe (n = 2 tissues per genotype). (**L, M**) Mg^{2+} levels in the serum (**L**) and bones (**M**). (**N**) 24 hr urinary Mg^{2+} excretion rate. Data are represented as mean±SEM. ***-$p \leq 0.001$; **-$p \leq 0.01$; *-$p \leq 0.05$; n.s. – not significantly different (Student's t-test); n – number of mice examined. Histological analysis in (**F**) and (**K**) was performed with n = 3 animals per group resulting in similar observations.

DOI: 10.7554/eLife.20914.014

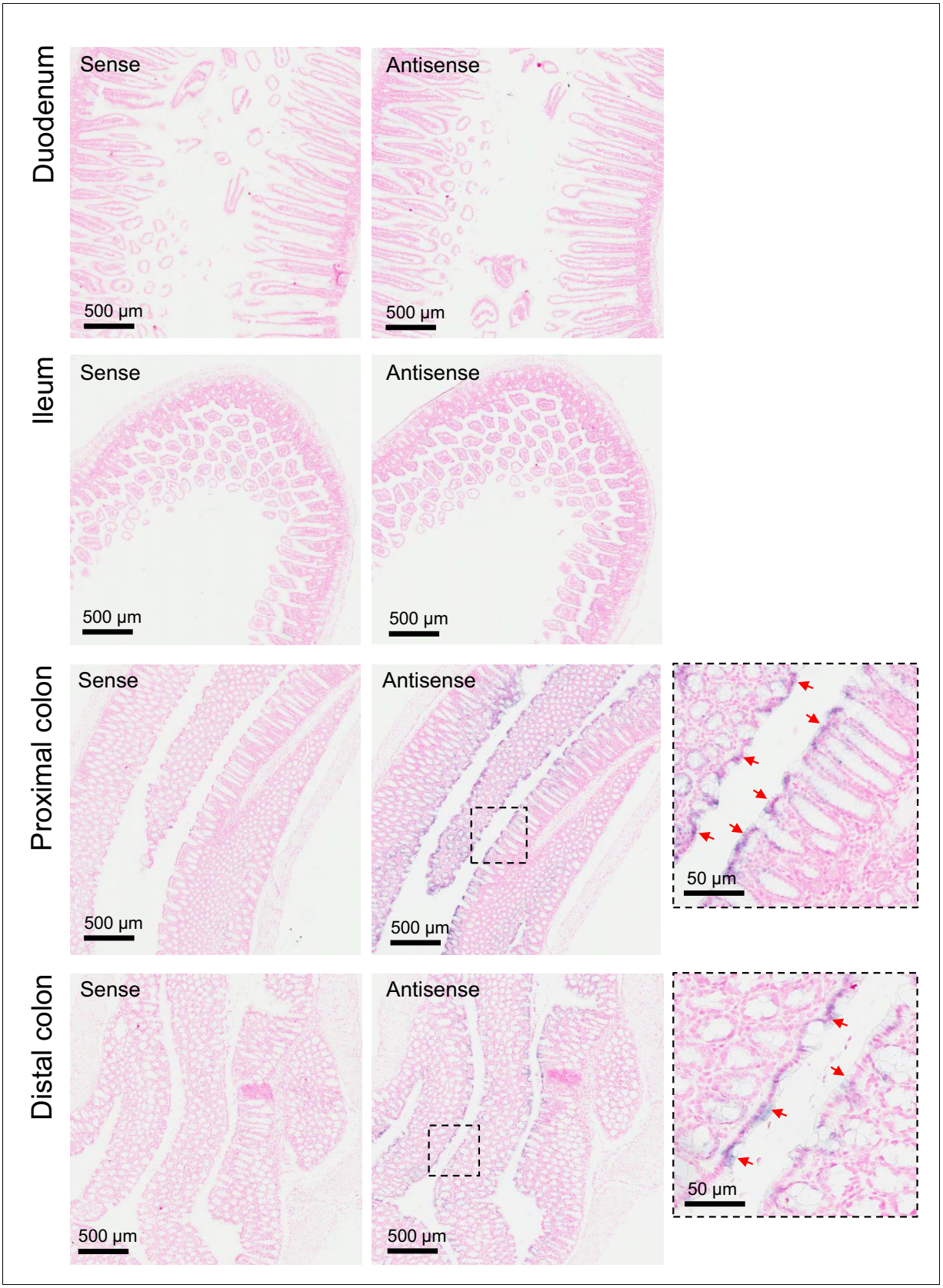

Figure 5—figure supplement 1. Expression pattern of *Trpm6* in the intestine. ISH on serial paraffin sections obtained from wildtype intestine using sense (left) and antisense (right) DIG-labelled probes for *Trpm6*. Boxes indicate the positions of the magnified images of the proximal and distal colon.

Figure 5—figure supplement 1 continued on next page

Figure 5—figure supplement 1 continued

Representative images of n = 3 tissues are shown. Arrows indicate *Trpm6*-positive cells in the colon. *Note: Trpm6* transcripts were not detectable in the duodenum and ileum and specifically present in the absorptive epithelium cells of the proximal and distal colon.

DOI: 10.7554/eLife.20914.015

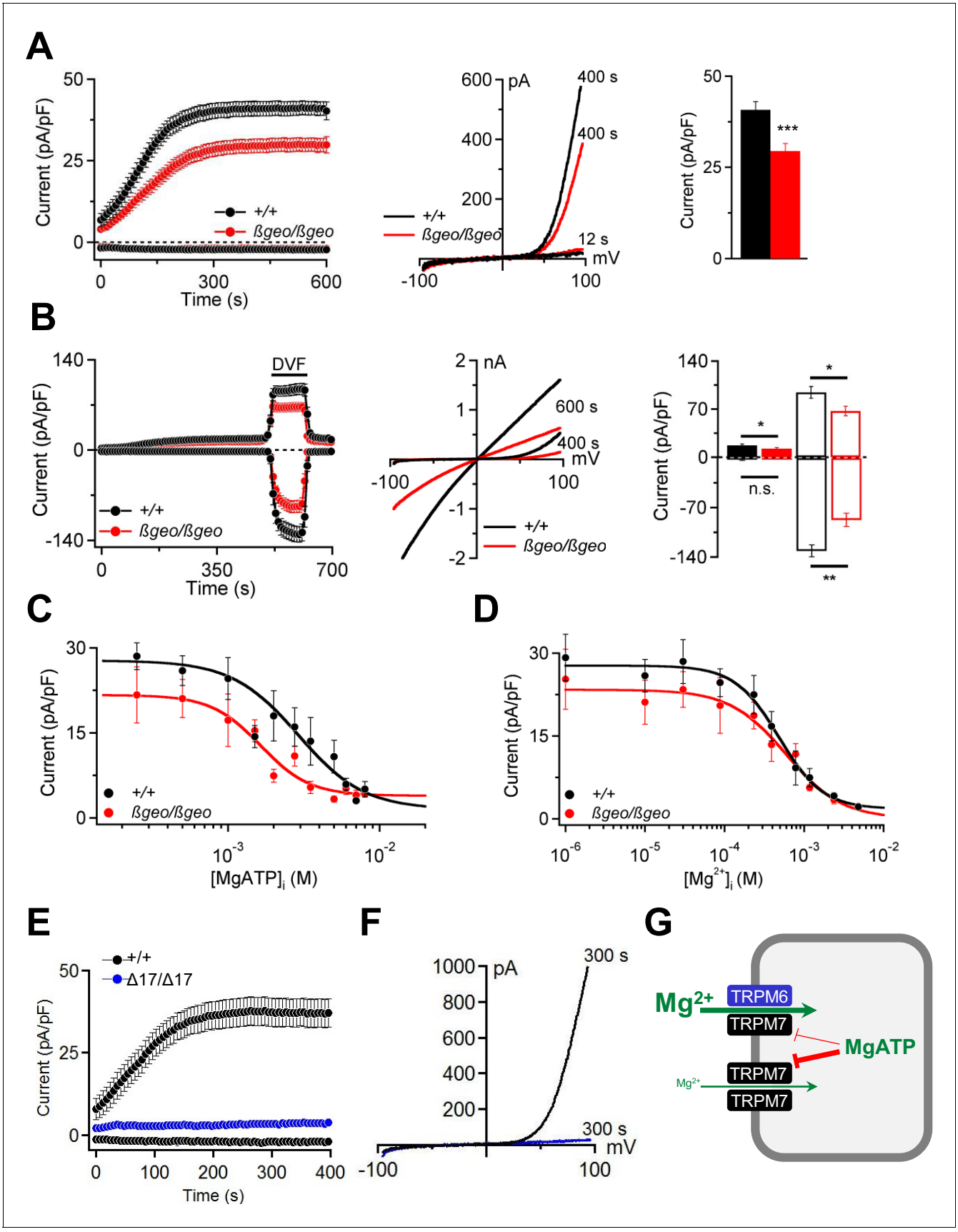
A
Current (pA/pF)
Time (s)
+/+
ßgeo/ßgeo
pA
400 s
12 s
mV
***
B
DVF
nA
600 s
n.s.
*
**
C
[MgATP]i (M)
D
[Mg2+]i (M)
E
Δ17/Δ17
F
300 s
G
Mg2+
TRPM6
TRPM7
MgATP

Figure 6. Characterization of TRPM6/M7-like currents in *Trpm6*- and *Trpm7*-deficient TS cells. (**A**) *Left panel:* Whole-cell currents measured at −80 mV and +80 mV over time in $Trpm6^{+/+}$ (n = 22) and $Trpm6^{\beta geo/\beta geo}$ (n = 22) TS cells. *Middle panel:* Representative current-voltage relationships obtained at 12 s and 400 s. *Right panel*: Bar graphs of current amplitudes at +80 mV (400 s). (**B**) Measurements were performed in control (n = 16) and *Trpm6*-deficient (n = 14) TS cells analogous to (**A**) except that the external saline (containing 2 mM Mg^{2+} and 1 mM Ca^{2+}) was exchanged with divalent-free (*DVF*) solution (black bar). *Right panel* shows currents measured before (filled bars) and after application of DVF solution (open bars) at 400 s and 600 s, respectively. (**C, D**) Dose-dependent inhibition of currents (+80 mV, 400 s) by $[MgATP]_i$ and $[Mg^{2+}]_i$, respectively (n = 4–18 cells per concentration). (**E, F**) Whole-cell currents of $Trpm7^{+/+}$ (n = 15) and $Trpm7^{\Delta 17/\Delta 17}$ (n = 10) TS cells studied similar to (**A, B**). Data are represented as mean±SEM. ***-p≤0.001; **-p≤0.01; *-p≤0.05; n.s. – not significantly different (Student's t-test). n – number of cells examined. (**G**) A suggested model for the molecular role of TRPM6 in epithelial cells.

DOI: 10.7554/eLife.20914.016

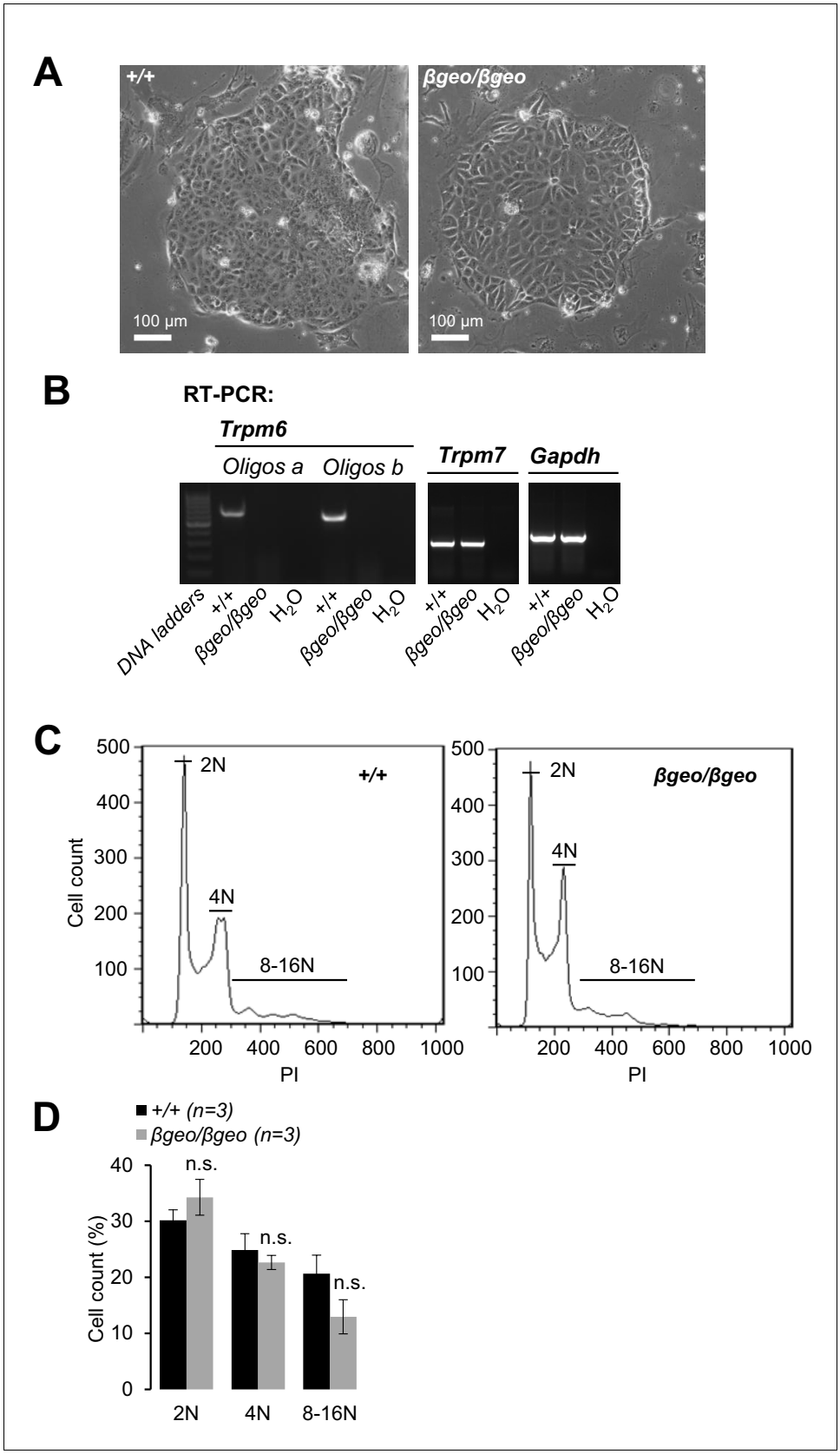

Figure 6—figure supplement 1. Characterization of *Trpm6*-deficient TS cells. (**A**) Phase-contrast images of *Trpm6*$^{+/+}$ (*+/+*) and *Trpm6*$^{\beta geo/\beta geo}$ (*βgeo/βgeo*) TS cells cultured in a regular cell culture medium. (**B**) Expression

Figure 6—figure supplement 1 continued on next page

Figure 6—figure supplement 1 continued

of *Trpm6* and *Trpm7* in TS cells assessed by RT-PCR. (**C, D**) Assessment of self-renewal of $Trpm6^{+/+}$ and $Trpm6^{\beta geo/\beta geo}$ cells. (**C**) Diploid (2N), tetraploid (4N), and polyploid (8–16N) DNA content was analysed by flow cytometry of $Trpm6^{+/+}$ and $Trpm6^{\beta geo/\beta geo}$ TS cells stained with propidium iodide (PI). (**D**) Bar graphs showing DNA contents (mean+/-SEM) calculated from three independent experiments outlined in (**A**). n.s. – not significantly different (Student's t-test). *Note:* 2N DNA content (diploid cells in G1), 4N (diploid cells in G2 or tetraploid cells in G1) and 8–16N (spontaneously differentiated polyploid trophoblasts) were not significantly altered in *Trpm6*-deficient TS cells indicating that self-renewal of $Trpm6^{\beta geo/\beta geo}$ cells was not affected.
DOI: 10.7554/eLife.20914.017

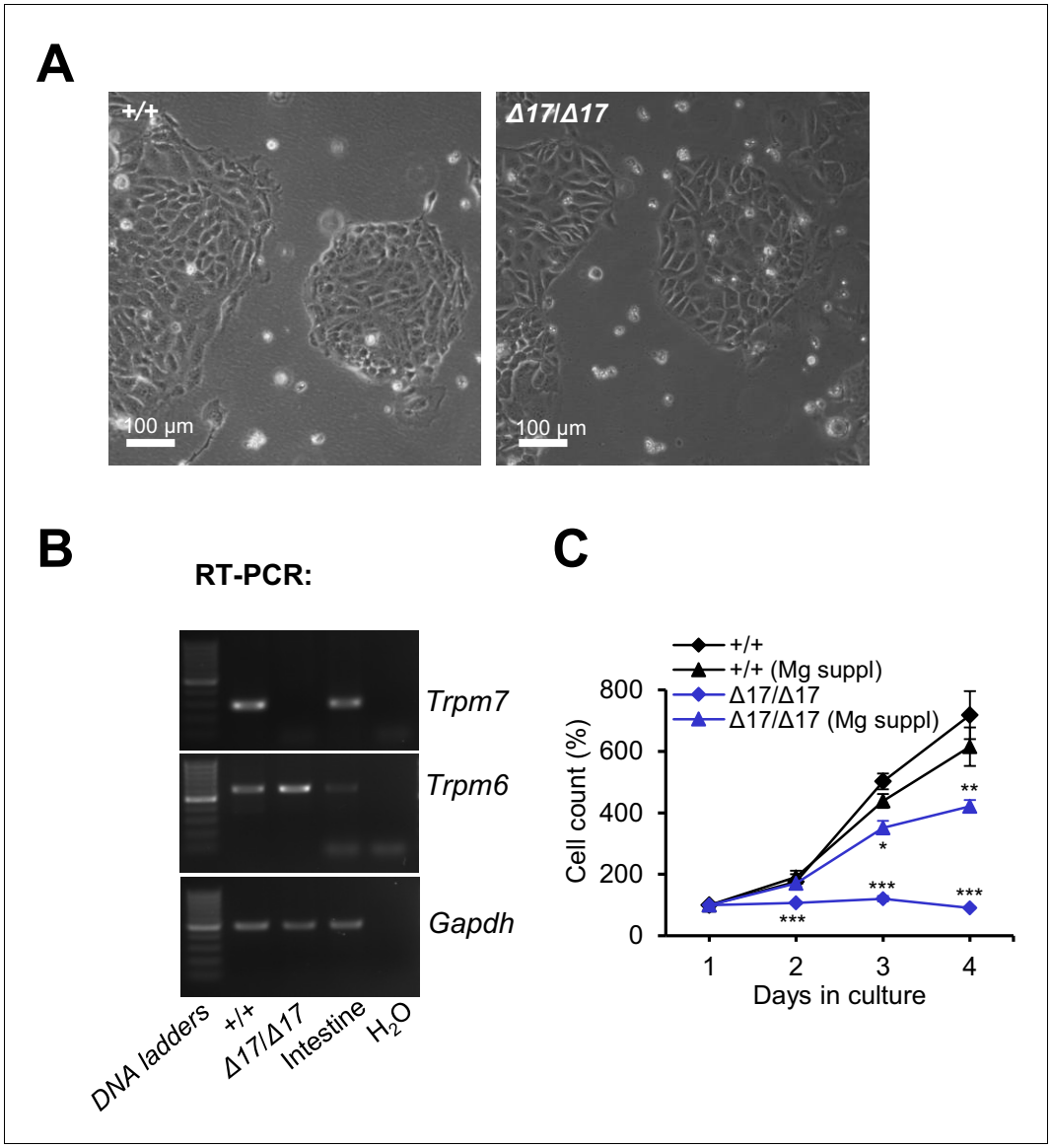

Figure 6—figure supplement 2. Examination of TS cells deficient in *Trpm7*. (**A**) Phase-contrast images of $Trpm7^{+/+}$ (+/+) and $Trpm7^{\Delta 17/\Delta 17}$ (Δ17/Δ17) TS cells cultured in a cell culture medium supplemented by 10 mM Mg^{2+}. (**B**) RT-PCR analysis of *Trpm7* and *Trpm6* in TS cells and mouse intestine (positive control). (**C**) Proliferation rate of $Trpm7^{+/+}$ (+/+) and $Trpm7^{\Delta 17/\Delta 17}$ (Δ17/Δ17) TS cells in standard and Mg^{2+} (10 mM) supplemented medium. The experiment was repeated three times. Student's t-test was applied for comparison of $Trpm7^{+/+}$ *versus* $Trpm7^{\Delta 17/\Delta 17}$ datasets.

DOI: 10.7554/eLife.20914.018

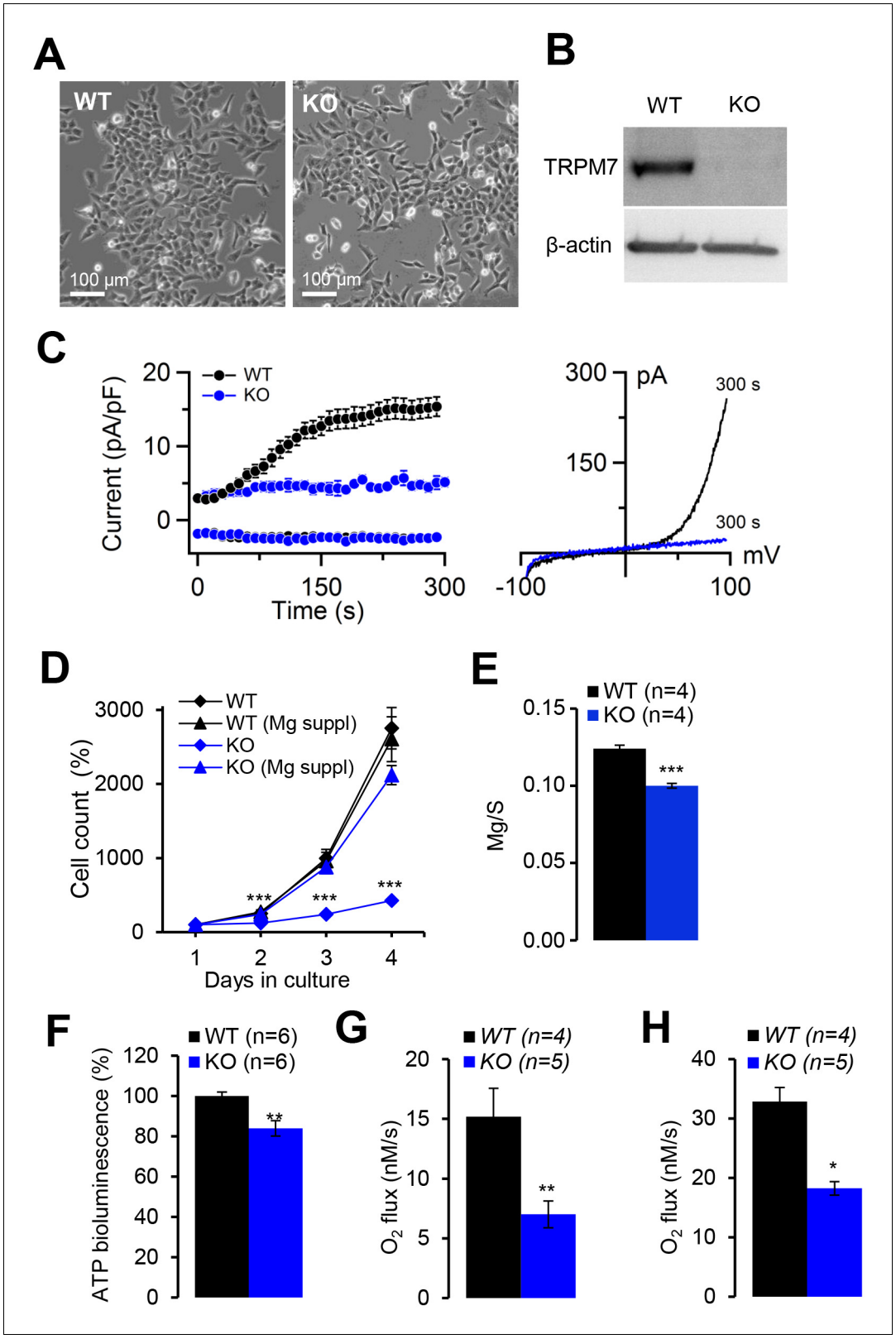

Figure 6—figure supplement 3. Evaluation of human haploid leukaemia (HAP1) cells deficient in *TRPM7*. (**A**) Phase-contrast images of parental (*WT*) and *TRPM7*-deficient (*KO*) HAP1 cells cultured in a cell culture medium supplemented with 10 mM Mg^{2+}. (**B**) Western-blot analysis of TRPM7 in WT and KO HAP1 cells. (**C**) Whole-cell

Figure 6—figure supplement 3 continued on next page

Figure 6—figure supplement 3 continued

currents in WT and KO HAP1 cells (determined as described in ***Figure 6***). *Left panel:* currents measured at −80 mV and +80 mV over time in WT (n = 9) and KO (n = 4) HAP1 cells. Data are represented as mean±SEM. *Right panel:* Representative current-voltage relationships obtained at 300 s. (**D**) Proliferation rate of WT and KO HAP1 cells either in standard or in Mg^{2+} (10 mM) supplemented medium. The experiment was repeated three times (n = 3). Data are represented as mean±SEM. Student's t-test was applied for comparison of the growth rates of WT *versus* KO cells cultured in standard medium (***-p≤0.001). (**E**) Determination of total Mg content in WT and KO HAP1 cells. Dried cell pellets (n = 4 for each genotype) were obtained from WT and KO HAP1 cells cultured for 24 hr in standard medium and analysed by ICP-MS. Elementary magnesium (Mg) content was normalized to sulfur (S) levels and represented as mean±SEM. ***-p≤0.001 (Student's t-test). (**F**) Assessment of total ATP levels in WT and KO HAP1 cells cultured for 24 hr in standard medium. ATP-induced luminescent of luciferase (CellTiter-Glo2.0 reagent) was normalized to a number of viable cells (Cell Counting Kit-8). The normalized luminescent signal in WT HAP1 cells was designated 100%. The experiment was repeated six times (n = 6). **-p≤0.01 (Student's t-test). (**G–H**) Routine respiration rate (**G**) and maximal respiration rate (**H**) analysed by Oxygraph-2k in WT and KO HAP1 cells cultured for 24 hr in standard cell culture medium (n – number of independent experiments).

DOI: 10.7554/eLife.20914.019

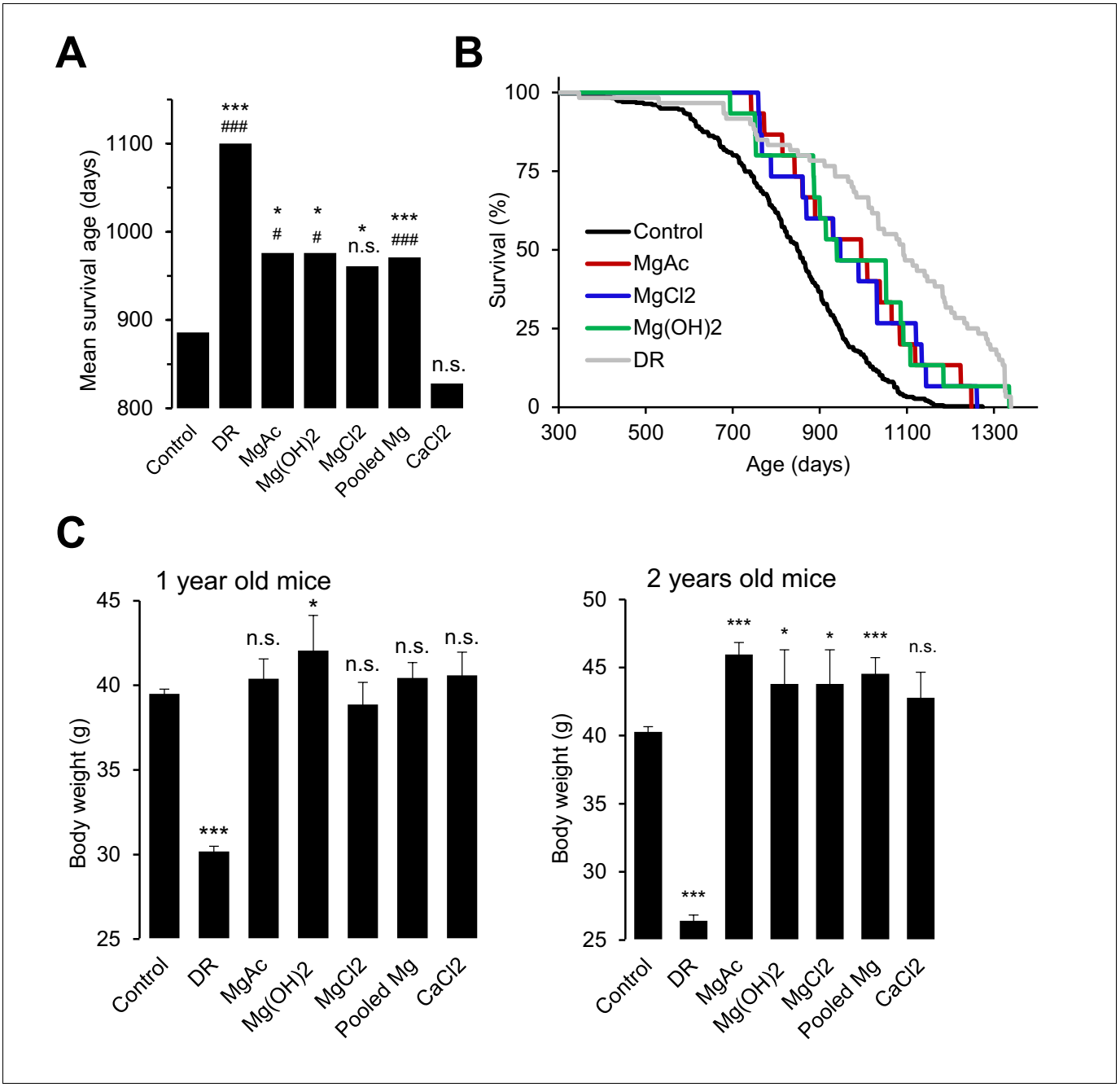

Figure 7. Effects of whole-life Mg^{2+} dietary treatments on B6C3F1 mouse strain. (**A**) Mean survival ages of B6C3F1 mice maintained at a control diet (*Control,* n = 335), under dietary restriction (*DR,* n = 60), or supplemented by $Mg(CH_3COO)_2$ (*MgAc,* n = 15), $Mg(OH)_2$ (n = 15), $MgCl_2$ (n = 15) and $CaCl_2$ (n = 15) in drinking water as outlined in ***Table 2***. *Pooled Mg* shows results for all Mg^{2+} supplemented mice pooled within a common group (n = 45). The obtained survival distributions were analysed by the MATLAB computing environment to calculate mean lifespans and corresponding P-values: ***-p≤0.001; **-p≤0.01; *-p≤0.05; n.s. – not significantly different. Alternatively, survival data of control mice versus individually treated groups were assessed by log-rank test: $^{###}$-p≤0.001; $^{##}$-p≤0.01; $^{#}$-p≤0.05; n.s. – not significantly different. (**B**) Kaplan-Meier survival distributions of B6C3F1 mice maintained on control diet (*Control*), Mg^{2+} supplemented groups (*MgAc, $MgCl_2$, $Mg(OH)_2$*) or mice under dietary restriction (*DR*). (**C**) Body weights (mean+/-SEM) of control and nutritionally fortified mice studied in (**A**). ***-p≤0.001; **-p≤0.01; *-p≤0.05; n.s. – not significantly different (one-way ANOVA). n – number of mice examined.

DOI: 10.7554/eLife.20914.020